Journal of Alloys and Compounds 511 (2012) 54–62

Contents lists available at ScienceDirect

Journal of Alloys and Compounds

journal homepage: www.elsevier.com/locate/jallcom

Electrical properties and temperature behavior of ZnO-doped PZT–PMnN modified piezoelectric ceramics and their applications on therapeutic transducers

Cheng-Che Tsai [a,*], Cheng-Shong Hong [b], Chia-Chi Shih [a], Sheng-Yuan Chu [c,d,**]

[a] Department of Electronics and Computer Science, Tung Fang Design University, Hunei District, Kaohsiung 829, Taiwan
[b] Department of Electronic Engineering, National Kaohsiung Normal University, Kaohsiung 824, Taiwan
[c] Department of Electrical Engineering, National Cheng Kung University, Tainan 701, Taiwan
[d] Advanced Optoelectronic Technology Center, National Cheng Kung University, Tainan 701, Taiwan

ARTICLE INFO

Article history:
Received 9 December 2010
Received in revised form 2 August 2011
Accepted 3 August 2011
Available online 30 August 2011

Keywords:
Tetragonality
Long-range order degree
Space charge
Effective coupling factor
Electro-acoustic efficiency

ABSTRACT

$Pb_{0.98}Ca_{0.01}Sr_{0.01}[(Mn_{1/3}Nb_{2/3})_{0.054}Cu_{0.006}–(Zr_{0.52}Ti_{0.48})_{0.94}]O_3$ (PMNCZT) + x wt.% ZnO (PMNCZT–Z10x) ceramics were prepared and sintered at a low temperature 980 °C, using the modified mixed-oxide method. The phase structure and microstructure evolutions were examined by XRD and SEM analyses. Effects of ZnO additives on the dielectric relaxation, piezoelectric, temperature stability, and ferroelectric properties were systematically investigated. The results showed that the ZnO doping increased the tetragonality ratio, tetragonal phase fraction, and long-range order degree of crystal structure. In addition, the electromechanical coupling factors, and the temperature stability of resonance frequency and resonant resistance were improved with increasing the ZnO amounts until $x = 1$. Beside these properties, the decrease of Q_m was related to decreasing in normalized change value of space charge. This developed compositions had k_p and k_t of 0.56 and 0.55, Q_m of 1280, d_{33} of 285 pC/N, $\varepsilon_{33}^T/\varepsilon_0$ of 980, tan δ of 0.0023, coercive field (E_c) of 11 kV/cm, and remnant polarization (P_r) of 28 μC/cm^2. Their corresponding transmission coefficient of intensity exhibited from value of 60.12% ($x = 0$) to value of 68.56% ($x = 2$) by the acoustic model calculation. To evaluate the dynamic performance of developed piezoceramics, a 3 MHz therapeutic transducer was fabricated using the trade-off ceramics with $x = 0.5$. Its properties exhibited that the average effective coupling factors k_{eff}^2 of 5.6%, electro-acoustic efficiencies of 34.1%, and dynamic acoustic power 0.75 W were better than those of a commercial transducer.

1. Introduction

Lead zirconate titanate (PZT) with the perovskite structure (general formula ABO_3) has the high electromechanical transformation properties near the morphotropic phase boundary (MPB) region which are applied in the fields of motors, transformers, and transducers [1–3]. To meet the requirements of applications, many aliovalent additions of the PZT network system occupying the A-site or B-site of crystal structure are made to induce the "soft" or/and "hard" effect for improving the piezoelectric activity (i.e., high mechanical coupling factor, K values) and decreasing the internal loss (i.e., high mechanical quality factor, Q values) during the electromechanical transformation. In lead-based $Pb[(Mn_{1/3}Nb_{2/3})_x–(Zr_{0.52}Ti_{0.48})_{1-x}]O_3$ (PMnN–PZT) piezoelectric material systems can be adapted to various power device applications. They have a high electromechanical coupling factor, high mechanical quality factor, high vibration velocity, lower dynamic aging rate, low nonlinear characteristic, and high remnant polarization, which make them suitable for high-performance devices [3–6].

In recent years, lead-free piezoelectric material systems have been developed and hoped to replace the PZT-based systems [7–9]. However, it is difficult to achieve a high electromechanical coupling factor (e.g., $k_p \geq 0.55$, $k_t \geq 0.48$), high mechanical quality factor ($Q_m > 1000$), and high reproducibility with a low sintering temperature (<1000 °C) for fabrication of multilayer devices in power applications. Therefore, the development of low-temperature-sintered PZT-based piezoelectric materials with good properties has become a main concern. Such concern has become increasingly important due to avoiding lead volatilization and environmental protection.

It is well known that the CuO dopant used as an additive to the native composition to form liquid phase compounds, and to enhance the sintering density of ceramics [10–13]. However, piezoelectric property degradation at low sintering temperature must be overcame to meet the devices requirements such as co-firing

* Corresponding author. Tel.: +886 7 6939626; fax: +886 7 6933406.
** Corresponding author. Tel.: +886 6 2757575x62381; fax: +886 6 2345482.
E-mail addresses: jjtsai@mail.tf.edu.tw, jertsai@seed.net.tw (C.-C. Tsai), chusy@mail.ncku.edu.tw (S.-Y. Chu).

0925-8388/$ – see front matter © 2011 Elsevier B.V. All rights reserved.
doi:10.1016/j.jallcom.2011.08.009

ceramic sheets with internal Ag or Cu metal electrode. Therefore, the co-doping effects of CuO and metal oxides (e.g., ZnO, SnO_2, MnO_2, etc.) has been used for lowering the sintering temperature and enhancing the piezoelectric properties in fabrication of low-temperature sintered piezoelectric ceramics.

Recently, the addition of micro scale ($d_{50} \sim 0.6$–$1.0\ \mu m$) or nano scale ($d_{50} < 100$ nm) ZnO into PZT-based and lead-free piezoelectric ceramics had attracted much attention for effectively promoting the electrical properties and the mechanical strength by the mixed-oxide method or sol–gel route. Ha et al. reported that the dielectric constant, electromechanical coupling factor, and piezoelectric charge coefficient can be enhanced by doping suitable ZnO [14]. Ahn et al. showed that ZnO was effective in improving the piezoelectric properties [15]. Yoon et al. showed that ZnO could enhance the piezoelectric voltage output coefficient (g_{33}) and piezoelectric charge constant (d_{33}) [16], Wang et al. reported that the ZnO nanowhisker could greatly improve the piezoelectric properties, mechanical strength and aging rate of PZT ceramics [17], and Zhao found the similar results from nano ZnO doping into the PZT thick-film by a hybrid sol–gel route [18]. Wongmaneerung et al. also showed that the suitable addition of ZnO nanowhiskers into PT ceramics could enhance the densification, mechanical and dielectric properties [19]. Similarly to lead-free piezoelectric ceramics, the nano ZnO addition had the same effects in enhancing the d_{33}, k_p and electric properties at a lower sintering temperature (<1070 °C) [20,21]. However, for considering the cost of nano ZnO powder intended to mass production, the addition of commercial particle (micro scale) ZnO into the PMNCZT based composition is our aim to study the dielectric relaxation in the diffusion phase transition (DPT), piezoelectric properties in the temperature stability, ferroelectric properties related to space charge variation, and their requirements on power device applications.

In our previous work, the low-temperature sintered CuO-doped $Pb_{0.98}Ca_{0.01}Sr_{0.01}\ [(Mn_{1/3}Nb_{2/3})_{0.06}(Zr_{0.52}Ti_{0.48})_{0.94}]O_3$ piezoelectric ceramics substrates for the SAW devices have been successfully developed and exhibited excellent characterization in the effective coupling factor of devices [22]. Recently, the mechanism of ZnO and CuO co-doping into the crystal structure of above-mentioned piezoceramics has been proposed by the enlarged XRD pattern shift and conductive analysis as reported in our paper [23]. On the other hand, the modified mixed-oxide method (wolframite method combined with mixed-oxide method) was used as a synthesis method in this paper. This method has been used in PZN–PZT based material systems with good dielectric and piezoelectric properties [24,25]. In the present study, the ZnO addition is tried to improve the electrical and temperature stability properties in the low-temperature-sintered PMNCZT ceramics system, using the modified mixed-oxide method. Simultaneously, the trade-off piezoelectric ceramics are applied to physiotherapy transducers whose performances are compared to those of the commercial transducers. According to the authors' knowledge, such investigation has rarely been conducted.

2. Experimental procedure

Following to our previous work, 1 mol% Ca and Sr dopants were added to improve the loss effects of the piezoelectric ceramics [22]. The compositions chosen in the present study were $Pb_{0.98}Ca_{0.01}Sr_{0.01}[(Mn_{1/3}Nb_{2/3})_{0.054}Cu_{0.006}-(Zr_{0.52}Ti_{0.48})_{0.94}]O_3$ (PMNCZT) + x wt.% ZnO (abbreviated as PMNCZT–Z10x), where x = 0, 0.1, 0.5, 1, 1.5, and 2. The excess 0.5 mol% of PbO was added to compensate for the lead loss during synthesis. Specimens were prepared with various compositions to improve the sintering density and obtain the optimum piezoelectric properties.

Commercially available oxide powders of PbO, $SrCO_3$, $CaCO_3$, Nb_2O_5, $MnCO_3$, ZrO_2, TiO_2, CuO, and ZnO with purities > 99% were used as the starting materials. The perovskite structure was prepared using the modified mixed-oxide method. The wolframite precursor $(Zr_{0.52}Ti_{0.48})O_2$ was first calcined at 1400 °C for 6 h. Then, Nb_2O_5, $MnCO_3$, $SrCO_3$, $CaCO_3$, CuO, PbO and $(Zr_{0.52}Ti_{0.48})O_2$ were weighed by mole ratio according to the given composition and ball-milled for 24 h. After being dried, the powders were calcined at 850 °C for 3 h. ZnO was added to the calcined powders, then ball-milled for 24 h and dried. The 8 wt.% of PB72 (a brand of commercial binder) and 40% distilled water, which formed the binder solution, were added to the dried powders and ball-milled, and then granulated. The samples were pressed into a disc 16 mm in diameter and 2.2 mm in thickness. The average green density formed was 5.5 g/cm^3. The samples were sintered at 930–1020 °C for 4 h in a covered alumina crucible. Then, the sintered pellets were polished to the desired thickness, screen-printed with silver paste on both faces, and then fired at 760 °C for 10 min. Then, the electroded samples were poled at a DC electric field of 3 kV/mm for 30 min in a 150 °C silicon oil bath.

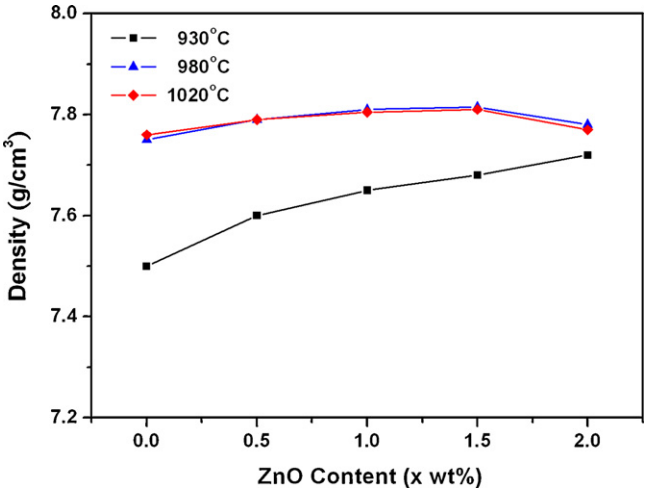

Fig. 1. Bulk density of the PMNCZT–Z10x ceramics as a function of ZnO content at different sintering temperature.

The bulk densities of the polished pellets were measured using the Archimedes method. Compositional analyses for the sintered pellets were determined by X-ray diffraction (XRD) using a Siemens D-5000 diffraction meter. The microstructure was analyzed by field emission scanning electron microscopy (FESEM) using Hitachi S-4100 meter. Elemental analysis was performed by environmental scanning electron microscopy (ESEM) equipped with energy dispersive spectrometer (EDS) using FEI Quanta 400F. The Curie point (T_c) and the dielectric properties of unpoled samples were measured with a HP-4192A impedance analyzer at 1 kHz, 10 kHz, and 100 kHz with 0.5-V_{rms} in a controlled furnace with a heating rate of 1 °C/min from 20 to 450 °C. To measure the piezoelectric properties, the poled specimens were aged for a week to obtain the stable values. Then, the resonance frequency, anti-resonance frequency and resonant resistance were measured by Agilent 4294A precision impedance analyzer. The mechanical quality factor and electromechanical coupling factor were measured using the resonance and anti-resonance method according to IEEE standards [26].

Ferroelectric P–E hysteresis loops were obtained using a modified Sawyer-Tower circuit under an ac field of 60 Hz at a maximum strength 5 kV/mm [27]. And, the piezoelectric charge coefficient d_{33} was measured with a using a wide-range d_{33} meter 90-2030 (APC International Ltd.).

After finishing the developed material compositions, the therapeutic transducer was fabricated using the proposed ceramics, as compared to the commercial therapeutic transducer. The acoustic power was measured by ultrasound power meter (model: UPM-DT-1 AV, Ohmic Instruments Co.).

3. Results and discussion

3.1. Physical properties

Bulk densities of ZnO-doped PMNCZT (PMNCZT–Z10x) specimens increase with increasing sintering temperature and amounts of ZnO shown in Fig. 1. The density of samples reaches the maximum value at x = 1.5 and then decreases for x > 1.5. When the sintering temperature is within 980–1020 °C, the bulk densities of ZnO-doped specimens respectively reach the maximum values between 7.82 g/cm^3 and 7.85 g/cm^3, which are higher than those of un-doped PMNCZT specimens. It is indicated that the density of samples saturates at the sintering temperature of 980–1020 °C. Therefore, the sintering temperature 980 °C is taken as the preferred temperature to achieve our goal for low-temperature-sintered PMNCZT–Z10x compositions. These results

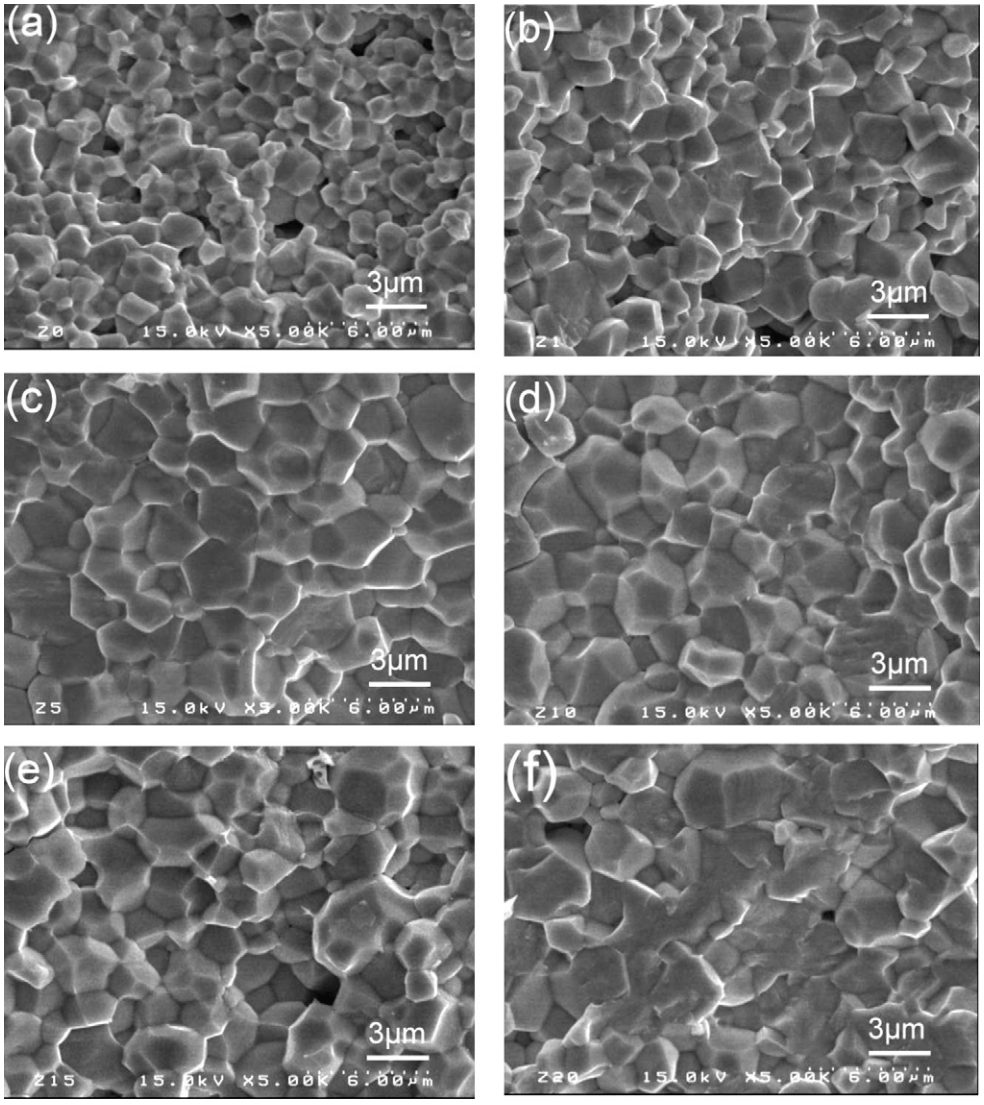

Fig. 2. SEM micrographs of the fractured specimens sintered at 980 °C for PMNCZT–Z10*x* composition with (a) $x = 0$, (b) $x = 0.1$, (c) $x = 0.5$, (d) $x = 1$, (e) $x = 1.5$, and (f) $x = 2$.

indicate that ZnO dopant can lower the sintering temperature and increase the sintering ability due to the additive of ZnO probably forming the low-melting point compound to expedite mass diffusion [28].

The SEM micrographs of ZnO-doped PMNCZT specimens are shown in Fig. 2. The grain size increases with increasing ZnO content, from 1.5 to 2 μm at $x = 0$ to 2–4 μm at $x = 1$, and then decrease for $x > 1$. This can be ascribed to suitable amounts of ZnO additive facilitating the grain growth and yields a dense structure for $0 \leq x \leq 1$. For $1 < x \leq 1.5$, the smaller amounts of ZnO will segregate at grain boundaries due to the limited solid solubility, inhibiting the grain growth resulting in the decrease of grain size. However, as $x > 1$, the more amounts of ZnO segregated at grain boundaries result in the abnormal grain growth and pores formation, presenting an inhomogeneous microstructures. This is due to the forming of the lower melting mixture of PbO, CuO, ZnO, MnO, and Nb_2O_5 (liquid phase) at grain boundaries. The EDX spectrum of 2 wt.% ZnO-doped PMNCZT ceramics (Fig. 3) shows that the amount of ZnO at the grain boundary (b) is higher than that at the grain particle (a). It can validate that the over-amount ZnO will segregate at grain boundaries and form the liquid phase with other metal oxides. And, this result is consistent with the findings reported by Li et al. [29] and Park et al. [28].

The XRD patterns of the ZnO-doped PMNCZT specimens ranging from 20° to 80° and enlarged (0 0 2) and (2 0 0) peaks within 42–48° sintered at 980 °C are shown in Fig. 4. As can be seen, no obvious second phase ($Pb_3Nb_4O_{13}$) is detected, but the crystal structures of the specimens slightly change after the addition of ZnO, as revealed by the incorporation change of the (0 0 2) and (2 0 0) peaks. The perovskite phase appears to co-exist with tetragonal and rhombohedral phases. It can be concluded that Zn ions exit mainly in the state of Zn^{2+} and most likely replace the B-site ions in the perovskite structure of the BO_6 octahedron. As a result, oxygen vacancies are formed leading to contraction of crystal structure. While the radius of Zn^{2+} is larger than that of B-site ion (ionic radius: $Zn^{2+} = 0.74$ Å, $Mn^{2+} = 0.67$ Å, $Nb^{5+} = 0.64$ Å, $Zr^{4+} = 0.72$ Å, and $Ti^{4+} = 0.605$ Å for CN = 6), the crystal structure leads to expansion. According to these two effects, the (0 0 2) and (2 0 0) peaks exhibit a slight shift toward the higher 2θ angle. This illustrates that the lattice constants are slightly decreased, while the tetragonality (c/a ratio) and tetragonal phase fraction (F_T) are enhanced with increasing ZnO content. They can be calculated by fitting the two Gaussian functions for the intensive overlap of the (2 0 0) including $(2\,0\,0)_T$ and $(2\,0\,0)_R$ in the 2θ range of 44–47° [30]. Detail results are listed in Table 1.

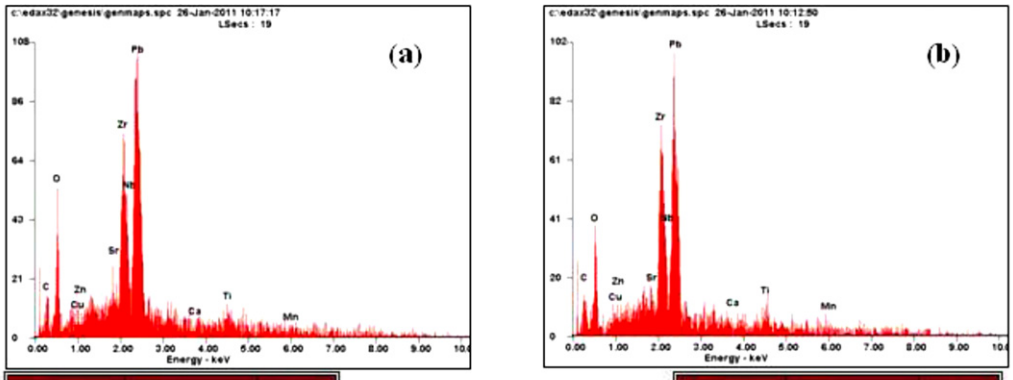

Element	Wt%	At%
CK	05.79	29.15
OK	05.37	20.29
CuL	01.20	01.15
ZnL	01.37	01.27
SrL	03.15	02.17
ZrL	19.50	12.93
NbL	08.83	05.74
PbM	42.84	12.50
CaK	02.05	03.10
TiK	04.94	06.23
MnK	04.97	05.47
Matrix	Correction	ZAF

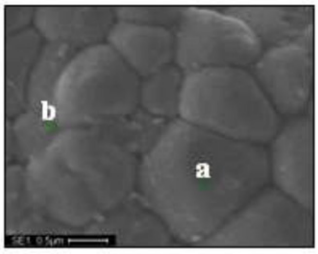

Element	Wt%	At%
CK	06.11	29.10
OK	06.22	22.27
CuL	01.30	01.17
ZnL	01.68	01.47
SrL	02.96	01.93
ZrL	20.86	13.09
NbL	06.02	03.71
PbM	41.17	11.37
CaK	01.90	02.71
TiK	05.77	06.90
MnK	06.01	06.26
Matrix	Correction	ZAF

Fig. 3. SEM and EDS spectrum of 2 wt.% ZnO-doped PMNCZT at the (a) grain particle, and (b) grain boundary.

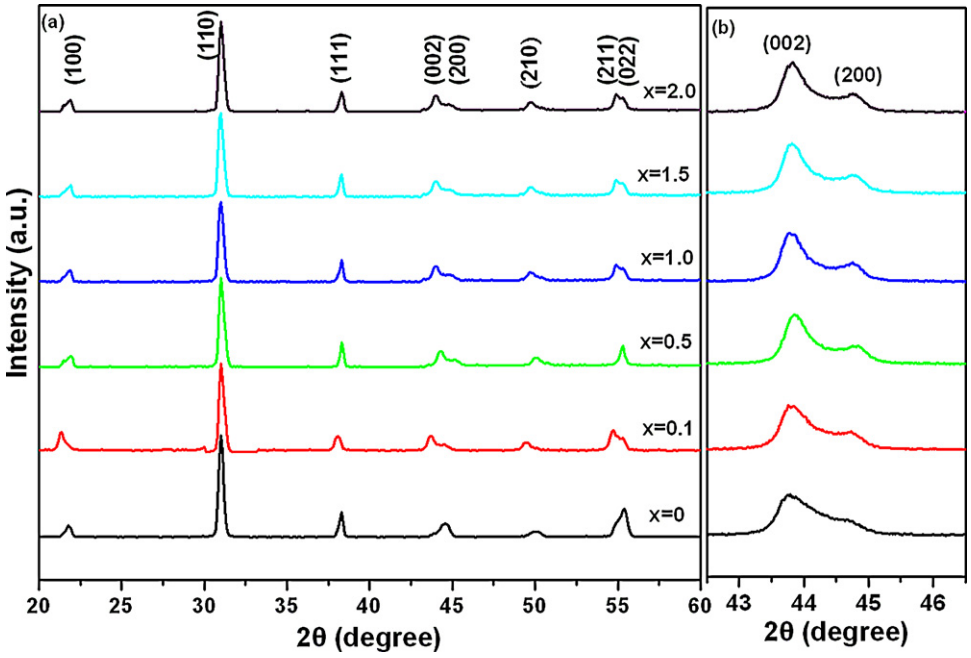

Fig. 4. X-ray diffraction patterns of the PMNCZT–Z10*x* specimens sintered at 980 °C (a) in the range of 20–80°, and (b) enlarged (0 0 2) and (2 0 0) peaks within 42–48°.

Table 1
Calculated fraction of the tetragonal phase (F_T%), the lattice constants (a and c) and tetragonality (c/a ratio) of the crystal structure, and the variation of $\varepsilon'_p - \varepsilon'_{up}/\varepsilon'_{up}$ for PMNCZT–Z10*x* specimens.

	ZnO (x) additive					
x (wt.%)	0	0.1	0.5	1	1.5	2
Fraction of tetragonal phase (F_T%)	72.6	75.3	79.4	79.6	79.1	78.8
Lattice parameter, a (Å)	4.0547	4.0478	4.0393	4.0461	4.0444	4.0438
Lattice parameter, c (Å)	4.1339	4.1339	4.1249	4.1321	4.1285	4.1285
c/a ratio of crystal structure	1.019	1.020	1.0212	1.0213	1.0207	1.0206
Variation of $\varepsilon'_p - \varepsilon'_{up}/\varepsilon'_{up}$ (%)	−8.4 1	−1.07	5.58	5.52	3.09	3.19

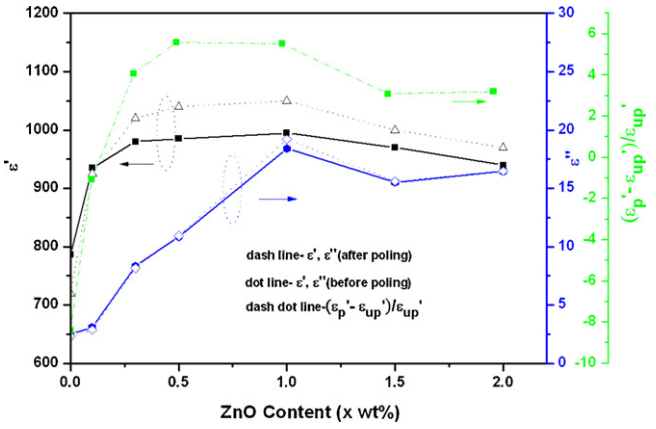

Fig. 5. Dielectric constant, loss tangent, and the variation of real dielectric constant for poled and un-poled specimens at frequency of 1 kHz versus the amount of ZnO for PMNCZT composition before and after poling, sintered at 980 °C.

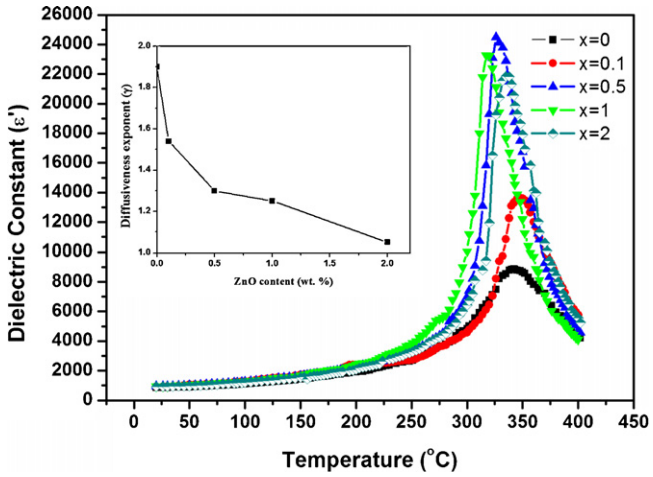

Fig. 6. Temperature dependence of dielectric constant measured at a 1 kHz as a function of ZnO for PMNCZT–Z10*x* composition sintered at 980 °C. (Inset is the diffusiveness exponent (γ) value at various ZnO contents for PMNCZT–Z10*x* composition.)

3.2. Dielectric properties

The real dielectric constant and imaginary dielectric constant of un-poled and poled specimens, designated as ε'_{up} and ε''_{up}, and ε'_{p} and ε''_{p} respectively, as a function of ZnO content in the PMNCZT–Z10*x* system sintered at 980 °C and measured at a frequency of 1 kHz are shown in Fig. 5. For the un-poled specimens, the real and imaginary dielectric constants increase with increasing ZnO content, achieving the maximum value at $x = 1$, and then decreasing for $x > 1$. These increases attribute to the increase of grain size with increasing amounts of ZnO additive, which lead to the increased polarizability (intrinsic contribution) and easily shifting domain wall motion (extrinsic contribution) resulting in both dielectric constant and dielectric loss increase [31–36]. For $1 < x < 1.5$, the amount of ZnO, exceeding the solid solubility, gradually segregates at the grain boundary to inhibit the grain growth resulting in the decrease of grain size leading to decreasing the dielectric constant and dielectric loss. With further increasing the ZnO content ($x > 1.5$), the pores form (Fig. 2(f)) due to the large grain impinge on each other, leading to the decrease of dielectric constant and the increase of dielectric loss. As a consequence, the dielectric constant and dielectric loss decrease due to the grain size decrease, while pores formation result in the dielectric loss increase [22,33]. In addition, it is indicated that the dielectric constant is correlated with the phase structure and the domain alignment. Thus, for poled specimens with the tetragonal structure, the dielectric constant of poled specimens is higher than that of un-poled specimens because dipolar polarizations are mainly enhanced by 180° domains wall contribution leading to increasing the dielectric constant. For poled specimens with the rhombohedral structure the dielectric constant of un-poled specimens is higher than that of the poled specimens, because the dipolar polarizations are decreased by the anisotropy effect (i.e., the spontaneous polarization direction [1 1 1] of rhombohedral structure is different from the poling direction [0 0 1] of specimens). The variation of real dielectric constant for poled and un-poled specimens ($\varepsilon'_{p} - \varepsilon'_{up}/\varepsilon'_{up}$) increases with ZnO addition, from −8.4% to 5.58% for $x \leq 1$ due to the c/a ratio and F_T increase. Similar results have been reported in the other piezoelectric material system [37,38]. For comparison, the fraction of the calculated tetragonal phase (F_T%), the c/a ratio of crystal structure. and the variation of ($\varepsilon'_{p} - \varepsilon'_{up}/\varepsilon'_{up}$) for PMNCZT–Z10*x* specimens are also shown in Table 1.

Fig. 6 shows the temperature dependence of the dielectric constant and diffusive phase transition around the Curie point at a measurement frequency of 1 kHz for PMNCZT–Z10*x* specimens. The dielectric constant peak of specimens at the Curie temperature, due to the ferroelectric–paraelectric phase transition, increases with increasing amounts of ZnO until $x = 0.5$. It attributes to the grain size increase [3,32]. With further increasing in ZnO amount, the dielectric constant peak decreases. It is attributed to some ZnO amounts, due to the solubility limited, probably being segregated at the grain boundary and clamping domain wall motion, resulting in a decrease of polarization [31]. The Curie temperature decreasing with the ZnO amount increasing until $x = 1$ for PMNCZT–Z10*x* specimens due to the ZnO substitution of B-site of perovskite structure [15]. And, further increasing x the Curie temperature increases due to some ZnO amount being segregated at the grain inhibiting the phase transformation resulting in the curie temperature increase. In addition, the degree of disorder or diffusiveness exponent (γ) for PMNCZT–Z10*x* specimens is estimated using the empirical formula $(1/\varepsilon) - (1/\varepsilon_m) = (T - T_m)^{\gamma}/C$ proposed by Uchino et al. [39]. The diffusiveness exponent (γ) value is calculated by the slope in the ratio of $\ln((1/\varepsilon) - (1/\varepsilon_m))$ and $\ln(T - T_m)$ through a linear curve fitting for

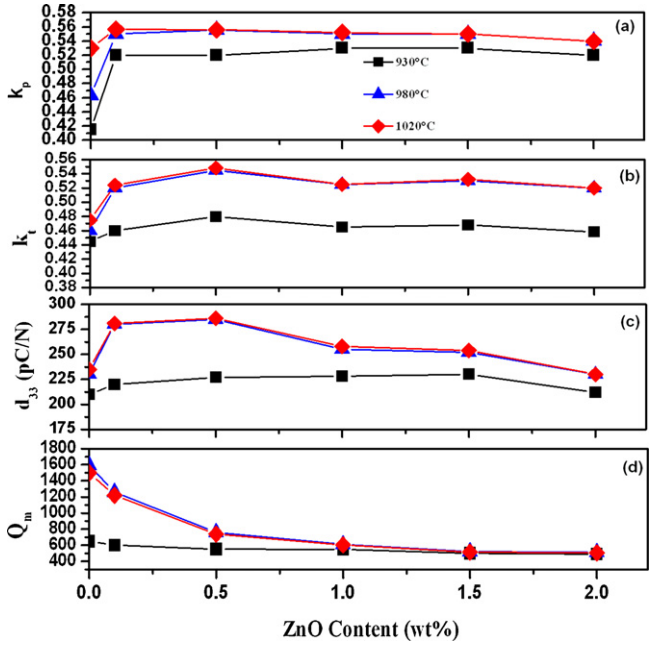

Fig. 7. Piezoelectric properties: (a) k_p, (b) k_t, (c) d_{33}, and (d) Q_m as a function of ZnO content for PMNCZT–Z10*x* composition at various sintered temperatures.

Table 2
Comparisons of properties of low-temperature sintered ZnO-doped PZT based piezoelectric ceramics.

Compositions	k_p	k_t	Q_m	$\varepsilon_{33}^T/\varepsilon_0$	d_{33}	T_c	
PMN–PZN–PZT + 0.1 wt.% Li_2CO_3 + 0.1 wt.% ZnO + 0.1 wt.% Pb_3O_4 (sintered at 995 °C)	0.6	–	1910	1032	–	–	[30]
0.41PNN–0.36PT–0.23PZ + 3 mol% ZnO (sintered at 950 °C)	0.53	–	60	3400	–	180	[14]
PMS–PZN–PZT + 0.6 wt.% WO3 + 0.2 wt.% MnO_2 + 0.1 wt.% ZnO (sintered at 1120 °C)	0.55		1899	–	–	270	[24]
PMS–PZT + 0.3wt.% ZnO (sintered at 1200 °C)	0.56	–	450	1727	–	–	[16]
APC841 + 0.2 wt.% CuO + 1.1 wt.% ZnO (sintered at 950 °C)	0.53	–	750	1337	–	280	[15]
PMnN–PZT + 0.15 wt.% CuO + 0.1 wt.% ZnO (sintered at 980 °C)	0.55	0.52	1280	980	285	340	Our samples

PMNCZT–Z10*x* specimens measured at 1 kHz as shown in the inset of Fig. 6. They indicate that the dielectric constant broaden around the curie point decreases with increasing ZnO amount in γ value from 1.88 ($x = 0$) to 1.02 ($x = 2$) due to increasing long-range order degree.

3.3. Piezoelectric properties

The piezoelectric properties of k_p, k_t, Q_m, and d_{33} for PMNCZT–Z10*x* specimens as a function of the amount of ZnO at various sintering temperatures are shown in Fig. 7. With increasing the sintering temperature, k_p, k_t, Q_m and d_{33} values of specimens increase and then reach the saturation at sintering temperatures 980–1020 °C. A suitable amount of ZnO can lower the sintering temperature and increase the grain size, resulting in easy domain wall motion [17].

As all specimens are sintered at preferred sintering temperature (980 °C), the values of k_p, k_t, and d_{33} initially increase with increasing ZnO contents, reach their maximum value 0.56, 0.54 and 290 at $x = 0.5$ and then drop for $x > 0.5$. The increasing values of k_p, k_t, and d_{33} are due to increasing the grain size and bulk density. With further increasing ZnO content ($x > 0.5$), the small amounts of ZnO probably segregate at the grain boundary resulting in decreasing k_p, k_t, and d_{33} [14]. These results are similar to CuO-doped PZT based hard piezoelectric materials [12,13]. While the Q_m values are decreased with increasing ZnO contents, the hard characteristics cannot be promoted because the electronegativity of B-cations (B–O bond covalence) and the crystalline structure might be responsible for the electric hardness of ZnO-doped PMNCZT

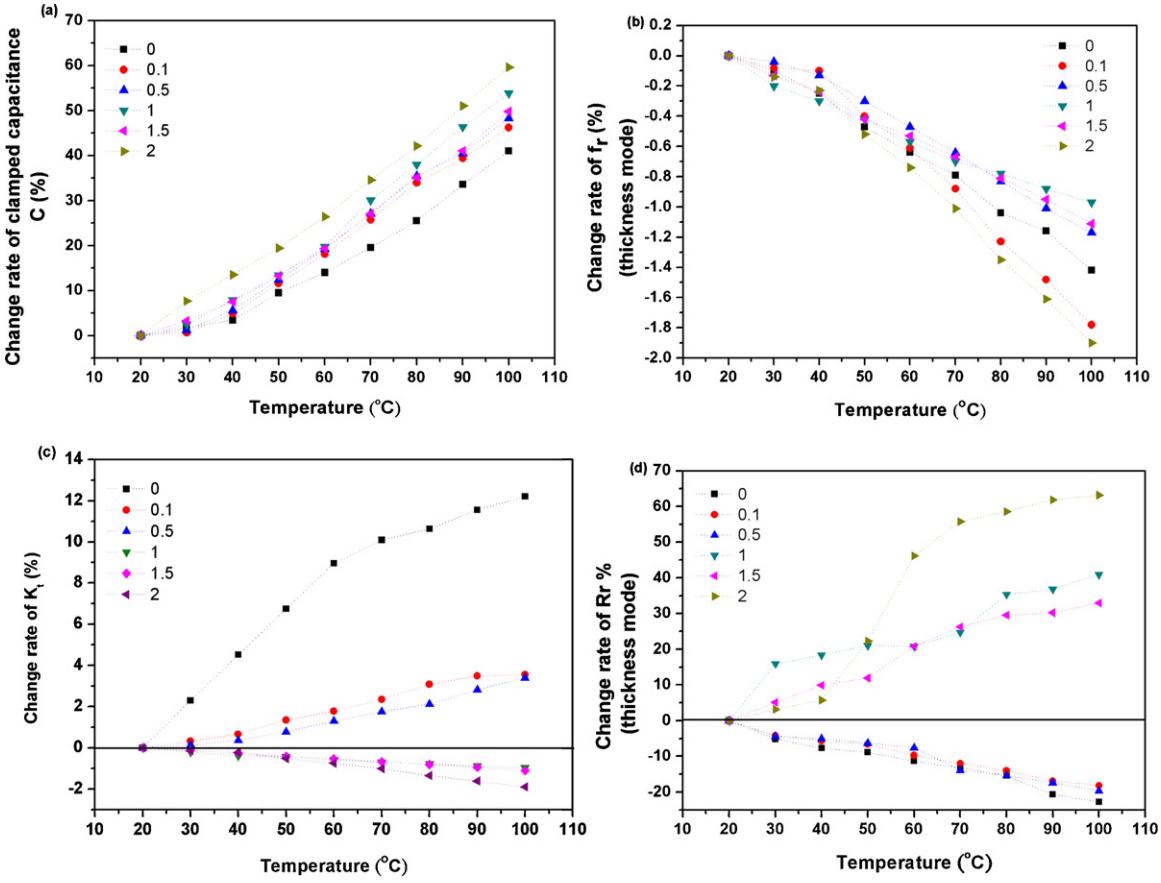

Fig. 8. Change rates of the (a) clamped capacitance, (b) thickness electromechanical coupling factor, (c) resonance frequency, and (d) resonance resistance as a function of temperature from 20 °C to 100 °C.

composition. A comparison of previously reported properties of low-temperature sintered ZnO-doped piezoelectric ceramics and those obtained in the present study is shown in Table 2.

3.4. Temperature stability properties

Power therapeutic transducers require good temperature stability of ceramics in change rate of the coupling factor (CRK_B), the resonance frequency (CRF_B), the resonance resistance (CRR_B), and the clamped capacitance (CRC_B) versus temperature. The relative studies had been discussed in our previous works [6,22] and other reports [40,41]. The value of the change rate is determined in the temperature range of t_1 to t_2 °C as follows:

$$\text{change rate of parameter } CRP_B = \frac{P_2(t_2) - P_1(t_1)}{P_1(t_1)} \times 100\%$$

where $P_2(t_2)$ and $P_1(t_1)$ are the measured or calculated parameters at temperatures t_2 and t_1, respectively. The change rate of parameters as a function of ZnO contents sintered at 980 °C ranging from 20 to 100 °C are shown in Fig. 8. Fig. 8(a) shows that the value of CRC_B increases with increasing ZnO amounts. The ZnO addition does not effectively improve the CRC_B values and the more addition of ZnO amounts ($x > 0.5$) presents the larger CRC_B with the temperature. This can be attributed to the loss tangent increasing with increasing ZnO amount and being thermally activated, which contribute most of the imaginary part of the dielectric constant and makes the dielectric constant increase as compared to un-doped specimen ($x = 0$).

Fig. 8(b) shows that the CRK_B with the addition of ZnO decreases for $x \leq 0.5$, and then becomes a negative value above 0.5 mol%. It is possibly that ZnO addition results in the larger change in CRK_B values due to increasing the bandwidth (the difference of anti-resonance frequency and resonance frequency) with the temperature rise for $x \leq 0.5$. While a high amount of ZnO ($x > 0.5$) results in CRK_B decreasing, it is due to domain wall motion being clamped since some ZnO contents possibly segregate at grain boundary.

Fig. 8(c) shows the CRF_B values in thickness mode as a function of temperature with various amount of ZnO. The absolute values of CRF_B greatly improved by increasing amount of ZnO (x) from the value of 1.9% ($x = 0$) to the minimum value of 0.8% ($x = 1.5$). The resonance frequency is correlated with the elastic compliance according to the formula $f_r = \frac{p}{2\pi r}\sqrt{1/s_{11}\rho(1-\sigma)}$ [42], where f_r is the resonance frequency, s_{11} is the elastic compliance, r is the radius, ρ is the bulk density, σ is poisson's ratio, and p is the lowest loot of equation expressed as $pJ_0(p) - (1-\sigma^E)J_1(p) = 0$. The resonance frequency is inversely proportional to the elastic compliance. As the composition with increasing ZnO contents, it induces the more tetragonal phase of MPB region as evidenced by Table 1, and the elastic compliance will be increased due to increasing grain size motion (extrinsic contribution) and the structure deformation (intrinsic contribution) [33]. As a result, the change rate of elastic compliance increases resulting in decreasing the change rate of resonance frequency. In other words, the larger elastic compliance change with temperature probably has the lower CRF_B value.

Fig. 8(d) indicates that the smallest absolute CRR_B value of 18% at $x = 0.1$ and that the value of CRR_B becomes the positive and presents the larger value greater than 25% for $x > 1$. This is attributed to a larger elastic compliance having a lower mechanical damping. The results of Fig. 8(c) and (d) indicate that a suitable amount of ZnO can improve both CRF_B and CRR_B, while the CRC_B is not improved due to the increased loss tangent corresponding increased polarizability with increasing amounts of ZnO.

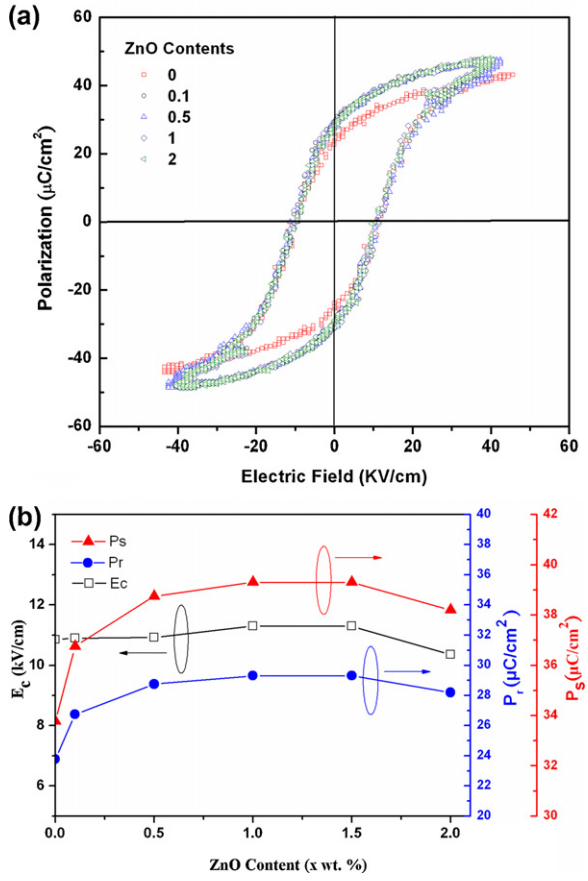

Fig. 9. (a) P–E hysteresis loop, and (b) the value of P_s, P_r and E_c of PMNCZT–Z10x specimens sintered at 980 °C as a function of ZnO content.

3.5. Ferroelectric properties

Fig. 9(a) shows the polarization–electrical field (P–E) hysteresis loops of PMNCZT–Z10x specimens with different ZnO amounts sintered at 980 °C. The hysteresis loops present the better square with increasing ZnO amounts. The trends of saturation polarization P_s (a nearly constant polarization value as E increases), the remnant polarization P_r (at $E = 0$), and the coercive field E_c (at $P = 0$) for PMNCZT–Z10x specimens are shown in Fig. 9(b), and their respective values are listed in Table 3. The values of P_s and P_r initially increase with increasing ZnO contents and achieve the maximum values 48.6 μC/cm² and 28.8 μC/cm², respectively, at $x = 0.5$. With further increasing ZnO amount except $x = 2$, the value of P_s and P_r presents a slight decrease in P_s and saturates in P_r. The E_c value exhibits a slight increase for $x \sim 0.5$, and then saturates for $x > 0.5$. The optimum ferroelectric properties are found at $x = 0.5$. Therefore, ZnO additive can increase P_r and E_c compared to those of PMNCZT specimens for $x \leq 0.5$. The former is due to tending toward a soft characteristic, and the latter is due to increasing the B-site vacancy. While the increase of the B-site vacancy resulted from ZnO doping does not enhance the hard characteristic, it is still unclear for this mechanism.

In addition, the reduced amount of space charge $(P_s - P_r)/P_s$ can explain the variation of Q_m from the hysteresis loop measurement [43,44]. To investigate this property, the value of Q_m and $(P_s - P_r)/P_s$ are listed in Table 3. It shows that the value of $(P_s - P_r)/P_s$ decreases with increasing the ZnO content, which is consistent with piezoelectric property of Q_m as a function of ZnO content (see Fig. 7(d)). The decrease of space charge correspondingly decreases

Table 3
Values of P_r, P_s, E_c, $(P_s - P_r)/P_s$ and Q_m for PMNCZT–Z10x for various amounts of ZnO.

Properties	ZnO additive (x wt.%)				
	0	0.1	0.5	1	2
E_c (kV/cm)	9.769	10.924	11.272	11.270	10.358
P_s (μC/cm^2)	42.573	48.102	48.654	46.998	46.998
P_r (μC/cm^2)	23.775	27.963	28.756	28.757	28.200
$(P_s - P_r)/P_s$	0.422	0.419	0.409	0.388	0.40
Q_m	1550	1280	800	720	600

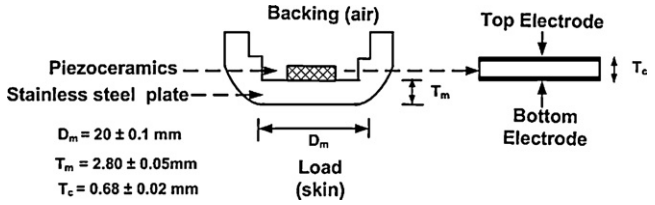

Fig. 10. Configuration of the 3 MHz therapeutic transducer.

the domain wall motion, which increases the electromechanical coupling factor (k) and the mechanical loss (Q_m^{-1}).

3.6. Therapeutic transducer fabrication and characterization

To evaluate the performance of PMNCZT–Z10x ceramics applied to physiotherapy applications, a 3 MHz air-backed therapeutic transducer (Fig. 10), comprising a stainless steel plate and piezoelectric ceramics, was fabricated. Its equivalent acoustic model is shown in Fig. 11. According to this model, the incident, reflected, and transmitted stresses and particle velocities are subject to continuity at the boundary. And, the transmission coefficient (T_E) of intensity can be expressed as follows [45]:

$$T_E = \frac{\text{transmitted energy}}{\text{incident energy}}\left(\frac{A_m}{A_c}\right)$$

$$= \frac{Z_c}{Z_L}\frac{4}{((Z_c/Z_L)+1)^2\cos^2 k_m t_m + (Z_c/Z_m + Z_m/Z_c)^2 \sin^2 k_m t_m}\left(\frac{A_m}{A_c}\right)$$

where k_m ($2\pi/\lambda_m$) is the wave number of ultrasound in metal plate, λ_m is the acoustic wavelength, Z_c is the acoustic impedance of the piezoelectric ceramic, Z_L (1.5 MRayl) and Z_b (441 Rayl) are the load (skin) and the air acoustic impedance respectively, A_c is the area of the ceramics, A_m is the area of the metal in contact with skin, and t_m is the thickness of the metal layer. The thickness of metal plate with $t_m = n \times (1/4)\lambda_m$ ($n = 1, 3, \ldots$) was designed to transmit the maximum ultrasound power. The calculated T_E for PMNCZT–Z10x ceramics is shown in Table 4. It shows that the T_E increases with increasing x content until $x = 1$.

To find the optimum composition for PMNCZT–Z10x ceramics, the requirements of high electromechanical coupling factor, good

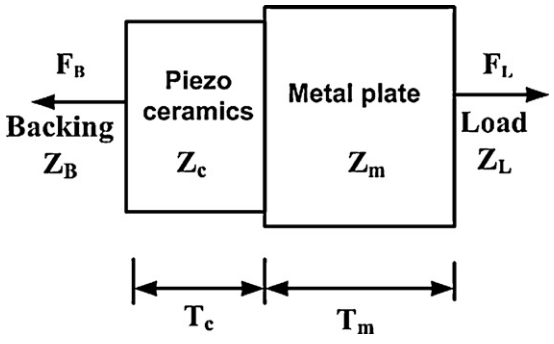

Fig. 11. Acoustic model of the air-backed ultrasonic transducer.

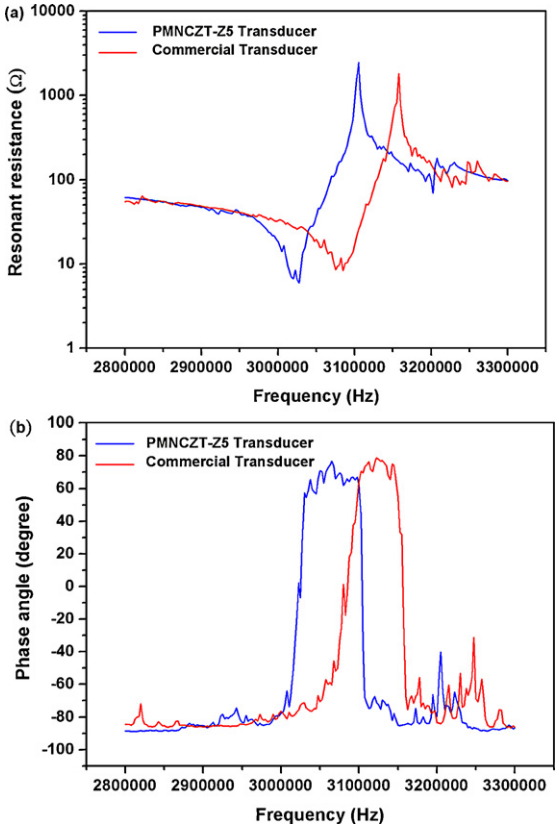

Fig. 12. (a) The impedance, and (b) phase angle of a 3 MHz therapeutic transducer as a function of frequency using PMNCZT–Z10x ceramics with $x = 0.5$ as compared to the commercial transducer (HES 3006).

temperature stability, and transmission coefficient are considered. The preferred composition chosen with $x = 0.5$ is used to fabricate the ceramic elements of therapeutic transducer.

Air-backed therapeutic transducer is fabricated using the PMNCZT–Z10x ceramics with $x = 0.5$, being adhered to the stainless steel plate using epoxy glue, and then being cured at a temperature of 120 °C for 1 h. This type of therapeutic transducer has a narrow bandwidth response because of mismatching acoustic impedance. To get the broad bandwidth of the transducer, one layer or multi-layer matching layer added between the ceramics and the metallic layer is required, achieving the acoustic impedance matching reported by Desilets et al. [46]. However, for physiotherapy applications, the narrow bandwidth of transducers is sufficient because the electromechanical vibration at the resonance frequency is only considered.

The frequency dependence of impedance and phase angle of the developed therapeutic transducer (PMNCZT–Z5 transducer) are evaluated and compared with a commercial therapeutic transducer (Model no.: HS 3040, manufactured by Hwang Sun Enterprise Co. Ltd.) as shown in Fig. 12(a) and (b). The developed therapeutic transducer exhibits the resonance resistance of 7.2 Ω, an effective

Table 4
Characterizations of PMNCZT–Z10*x* specimen used as the therapeutic transducer with various ZnO content.

PMNCZT–Z10*x* composition	Longitudinal velocity (m/s)	Density (kg/m^3)	Acoustic impedance, Z_c (MRayl)	Transmission coefficient, T_E	Electromechanical coupling factor, k_t
$x=0$	3798	7450	28.30	60.12	0.46
$x=0.1$	3866	7840	30.31	68.24	0.50
$x=0.5$	3896	7780	30.31	68.24	0.54
$x=1$	3975	7710	30.65	69.62	0.49
$x=2$	3916	7760	30.39	68.56	0.50

Table 5
Properties of PMNCZT–Z5 therapeutic transducers fabricated using the developed ceramics compared to those of commercial therapeutic transducer manufactured by HES Co. Ltd.

	Resonance frequency (MHz)	Resonance resistance (Ω)	Effective coupling factor, k^2_{eff}	Mechanical quality factor, Q_m	Dynamic electrical power (W)	Dynamic acoustic power (W)
Commercial transducer[a]	3.085	9.82	0.045	30	2.2	0.70
PMNCZT–Z5 transducer[b]	3.030	7.58	0.050	28	2.2	0.75

[a] Commercial transducer fabricated using PMnN–PZT ceramics.
[b] PMNCZT–Z5 transducer fabricated using low-temperature sintered PMNCZT–Z5 ceramics (our samples).

coupling factor k^2_{eff} of 5.6%, a bandwidth (BW) of 100 kHz, an acoustic power of 0.75 W under an input electrical power of 2.2 W, and an electro-acoustic efficiency of 34.1%, which are superior to those of the commercial therapeutic transducer. Comparison of property of the therapeutic transducer is listed in Table 5. These results show that the developed low-temperature sintered piezoelectric ceramics are suitable for fabricating high-frequency therapeutic transducers.

4. Conclusions

Piezoelectric ceramics with compositions of PMNCZT–Z10*x* sintered 980 °C were prepared by the modified mixed-oxide method. The properties of developed low-temperature-sintered piezoelectric ceramics could be tuned by suitable addition of ZnO content, and exhibit enhanced electromechanical transformation properties and good temperature stability of change rate of resonance frequency and resonance resistance in thickness mode vibration within $x=0.1$–0.5. However the mechanical quality factor is not improved. In addition, the dielectric constant broaden around the Curie point decreased with increasing ZnO content with γ from value of 1.88 ($x=0$) to value of 1.02 ($x=2$) due to increasing long-range order degree of ZnO-doped PMNCZT compositions. The Q_m decreases with decreasing the normalized space charge variations. Besides these properties, the corresponding transmission coefficient of intensity with ZnO content was calculated and exhibited from value of 60.12% ($x=0$) to value of 68.56% ($x=2$) by the acoustic model. Further, 3 MHz therapeutic transducers were successfully fabricated using the developed ceramics with $x=0.5$. Their effective coupling factor k^2_{eff} of 5.6% and electro-acoustic efficiency of 34.1% were better than those of commercial transducers.

References

[1] B. Jaffe, W.R. Cook Jr., H. Jaffe, Piezoelectric Ceramics, Academic Press Limited, New York, 1971.
[2] J.F. Tressler, S. Alkoy, R.E. Newnham, J. Electroceram. 2 (1998) 257–272.
[3] C.C. Tsai, T.K. Chiang, S.Y. Chu, IEEE Trans. Ultrason. Ferroelect. Freq. Contr. 56 (2009) 156–166.
[4] M. Takahashi, N. Tsubouchi, M. Yonezawa, T. Ohno, T. Akashi, NEC Res. Develop. 20 (1974) 57–66.
[5] H. Chen, X. Guo, Z. Meng, Mater. Chem. Phys. 75 (2002) 202–206.
[6] Q. Ise, K. Satoh, Y. Mamiya, Jpn. J. Appl. Phys. 38 (1999) 5531–5534.
[7] Y. Hiruma, T. Watanabe, H. Nagata, T. Takenaka, Jpn. J. Appl. Phys. 47 (2008) 7659–7663.
[8] T. Lee, K.W. Kwok, H.L. Li, H.L.W. Chan, Sens. Actuators A 150 (2009) 267–271.
[9] M. Guo, X.P. Jiang, K.H. Lam, S. Wang, C.L. Sun, Helen, L.W. Chan, X.Z. Zhao, Rev. Sci. Instrum. 78 (2007), art. no. 016105.
[10] D.W. Kim, K.H. Ko, K.S. Hong, J. Am. Ceram. Soc. 84 (2001) 1286–1290.
[11] Y.D. Hou, M.K. Zhu, H. Wang, B. Wang, H. Yan, C.S. Tian, Mater. Sci. Eng. B 110 (2004) 27–31.
[12] C.C. Tsai, S.Y. Chu, C.H. Lu, IEEE Trans. Ultrason. Ferroelect. Freq. Contr. 56 (2009) 660–668.
[13] X. Chao, D. Ma, R. Gu, Z. Yang, J. Alloys Compd. 491 (2010) 698–702.
[14] J.Y. Ha, J.W. Choi, C.Y. Kang, D.J. Choi, H.J. Kim, S.J. Yoon, Mater. Chem. Phys. 90 (2005) 396–400.
[15] C.W. Ahn, H.C. Song, S. Nahm, S. Priya, S.H. Park, K. Uhino, H.G. Lee, H.J. Lee, J. Am. Ceram. Soc. 89 (2006) 921–925.
[16] M.S. Yoon, Y.M. Kim, S.Y. Kweon, T.W. Hong, Y.G. Lee, S.L. Ryu, H.J. Kim, S.C. Ur, J. Electroceram. 18 (2007) 73–75.
[17] D.W. Wang, M.S. Cao, J. Yuan, R. Lu, H.B. Li, Q.L. Zhao, D.Q. Zhang, J. Alloys Compd. 509 (2011) 6980–6986.
[18] Q.L. Zhao, M.S. Cao, J. Yuan, W.L. Song, R. Lu, D.W. Wang, D.Q. Zhang, J. Alloys Compd. 492 (2010) 264–268.
[19] R. Wongmaneerung, S. Choopan, R. Yimnirun, S. Ananta, J. Alloys Compd. 509 (2011) 3547–3552.
[20] H.T. Li, B.P. Zhang, M. Cui, W.G. Yang, N. Ma, J.F. Li, Curr. Appl. Phys. (2011), doi:10.1016/j.cap.2010.12.026.
[21] R. Hayati, A. Barzegar, Mater. Sci. Eng. B 172 (2010) 121–126.
[22] C.C. Tsai, S.Y. Chu, C.K. Liang, J. Alloys Compd. 478 (2009) 516–522.
[23] C.C. Tsai, S.Y. Chu, C.S. Hong, S.F. Chen, J. Eur. Ceram. Soc. 31 (2011) 2013–2022.
[24] S. Nabunmee, G. Rujijanagui, N. Vittayakom, D.P. Cann, J. Appl. Phys. 102 (2007), art. no. 094108.
[25] N. Vittayakom, C. Puchmark, G. Rujijanagui, X. Tan, D.P. Cann, Curr. Appl. Phys. 6 (2006) 303–306.
[26] IEEE Standard on Piezoelectricity ANSI/IEEE Standard 176-1987, The Institute of Electrical and Electronics Engineers, New York, 1987.
[27] C.B. Sawyer, C.H. Tower, Phys. Rev. 35 (1930) 269–275.
[28] S.H. Park, C.W. Ahn, S. Nahm, J.S. Song, Jpn. J. Appl. Phys. 43 (8B) (2004) L1072–L1074.
[29] H. Li, Z. Yang, L. Wei, Y. Chang, Mater. Res. Bull. 44 (2009) 638–643.
[30] M.K. Zhu, P.X. Lu, Y.D. Hou, H. Wang, H. Yan, J. Mater. Res. 20 (2005) 2670–2675.
[31] K. Okazaki, K. Nagata, J. Am. Ceram. Soc. 56 (1973) 82–86.
[32] H.T. Martirena, J.C. Burfoot, J. Phys. C: Solid State Phys. 7 (1974) 3182–3192.
[33] C.A. Randall, N. Kim, J.P. Kucera, W. Gao, T.R. Shrout, J. Am. Ceram. Soc. 81 (1998) 677–688.
[34] G.M. Zhang, W.Y. Pan, S.J. Jang, L.E. Cross, J. Appl. Phys. 64 (1988) 6445–6451.
[35] G.M. Zhang, H. Wang, N. Kim, L.E. Cross, J. Appl. Phys. 75 (1994) 454–459.
[36] D.A. Ochoa, J.E. Garcia, R. Perez, A. Albareda, IEEE Trans. Ultrason. Ferroelectr. Freq. Contr. 55 (2008) 2732–2736.
[37] J.C. Shaw, K.S. Liu, I.N. Lin, J. Am. Ceram. Soc. 78 (1995) 178–182.
[38] G. Feng, R. Hong, J. Liu, Z. Li, C.-S. Tian, Ceram. Int. 35 (2009) 1863–1869.
[39] K. Uchino, S. Nomura, Ferroelectric 44 (1982) 53–61.
[40] R. Zhang, Z. Yang, X. Chao, C. Kang, Ceram. Int. 35 (2009) 199–204.
[41] X. Chao, Z. Yang, M. Donga, G. Li, Sens. Actuators A 151 (2009) 71–76.
[42] A.H. Meitzler, H.M. O'Bryan Jr., J. Am. Ceram. Soc. 55 (1972) 504–506.
[43] M. Takahashi, Jpn. J. Appl. Phys. 9 (1970) 1236–1246.
[44] S. Takahashi, M. Takahashi, Jpn. J. Appl. Phys. 11 (1972) 31–35.
[45] H.J. Pain, The Physics of Vibrations and Waves, 6th ed., John Wiley and Sons Ltd., England, 2005.
[46] C.S. Desilets, J.D. Fraser, G.S. Kino, IEEE Trans. Ultrason. Ferroelectr. Freq. Contr. su-25 (1978) 115–125.